Quantum Frontiers
上海交通大學 SHANGHAI JIAO TONG UNIVERSITY 李政道研究所 Tsung-Dao Lee Institute

ORIGINAL ARTICLE Open Access

A fully-connected three-user quantum hyperentangled network

Yiwen Huang[1†], Yuanhua Li[1,2†], Zhantong Qi[1], Yilin Yang[1], Yuanlin Zheng[1,3] and Xianfeng Chen[1,3,4*]

Abstract

Exploiting the fantastic features of quantum mechanics, a hyperentangled quantum network encoded in multiple degree of freedoms (DOF), e.g., polarization and orbital angular momentum DOFs, can encode more qubits per transmitted photon and offers a promising platform for many dramatic applications. Here, we demonstrate such a hyperentangled multiuser network with a fully connected network architecture by using dense wavelength division multiplexing and entanglement transfer technique. Three hyperentangled states in polarization and time-energy DOFs are multiplexed to three single mode fibers to form the fully connected network architecture. Then, three interferometric quantum gates are utilized for transferring quantum entanglement from time-energy to orbital angular momentum DOF. The experimental results reveal a high quality of the hyperentanglement of the constructed network with the entangled state fidelity of higher than 96%. Our approach can provide a novel way to construct a large-scale hyperentangled network that can support various kinds of quantum tasks like superdense coding and teleportation.

Keywords: Polarization entanglement, Time-energy entanglement, Orbital angular momentum, Entanglement transfer, Hyperentangled quantum network

1 Introduction

As the intriguing quantum mechanical characteristic, quantum entanglement is at the very heart of many quantum-information tasks [1–4], such as quantum repeaters [5], teleportation [6, 7], entanglement swapping [8, 9], quantum key distribution (QKD) [10–12], quantum secure direct communication (QSDC) [13], and quantum steering [14]. Thus far, as the quantum information technology has gradually reached a mature level [15–17], how to realize a large-scale quantum communication network effectively has become a thriving research field [18–20]. Entanglement based quantum network offers the promise platform for many dramatic applications, such as distributed quantum computation [21], quantum sensing [22], multiuser QKD [23], and free-space QSDC [24, 25]. Experimental advances in entanglement-based quantum technique lays the foundation for constructing a fully connected quantum Internet, which may revolutionize the way of information exchange in the future. Recently, the fully connected quantum communication network based on quantum entanglement has attracted much attention in constructing a large-scale metropolitan network [26–28]. Such type of network configuration enables multi users' communication with each other at the same time when minimizes the infrastructure and hardware.

In a future quantum network, quantum processor could enable heterogeneous quantum nodes to establish an encryption key with each other, relying on quantum entanglement encoded in various DOFs, such as orbital angular momentum (OAM), polarization, and time-energy. To date, there are already several categories of fully connected network encoded in single DOF, such as polarization [26, 27], time-energy [11] and time bin [29]. Among

*Correspondence: xfchen@sjtu.edu.cn
[1]State Key Laboratory of Advanced Optical Communication Systems and Networks, School of Physics and Astronomy, Shanghai Jiao Tong University, Shanghai 200240, China
[3]Shanghai Research Center for Quantum Sciences, Shanghai 201315, China
Full list of author information is available at the end of the article †Equal contributors

these DOFs, the technique of polarization entanglement has reached a mature level, and polarization-entangled states have played an important role in quantum communication [30–32] and quantum computation [33]. Recently, OAM entanglement has attracted much attention due to its unique characteristic in phase intensity profile and the fantastic feature of high dimension [34–36]. Moreover, hyperentanglement in multiple DOFs enables significant enhancement of information capacities and has stimulated new quantum protocols [37]. The higher data capacity and stronger error resilience make it an attractive candidate for many quantum-secure information processing such as dense coding [31, 32], entanglement distillation [38], and superdense teleportation [39]. Hyperentanglement in polarization and OAM DOFs has great potential for long-distance quantum information applications. A multiuser fully connected network based on hyperentanglement in polarization and OAM would provide a promising platform that can support the end users perform multiple quantum tasks [40]. However, the implementation of an OAM entanglement-based multiuser network is still challenging, mostly owing to the difficulty of preparing multi-channel OAM entangled states. How to flexibly construct a hyperentangled network in polarization and OAM DOFs become an important issue for constructing a multi-function quantum network.

Here, we proposed a hyperentangled multiuser network with a fully connected network architecture encoded in polarization and OAM DOFs. By using a polarization entangled source and dense wavelength division multiplexing (DWDM) technique, three hyperentangled states in polarization and time-energy DOFs are multiplexed to three single mode fibers to form the fully connected network architecture. Then, three interferometric quantum gates consisting of a Mach-Zehnder interferometer (MZI) with spiral phase plates (SPP) inserted in different paths are utilized for transferring quantum entanglement from time-energy to OAM DOF. The two-photon interference visibility is measured to be higher than 95% for both polarization and OAM entanglement, revealing a high quality of hyperentanglement in these two DOFs of the constructed network. Our approach can provide a novel way to construct a large-scale hyperentangled network and is expected to play important roles in long-distance quantum communication.

2 Construction of the network architecture

The topology architecture of the hyperentangled network can be interpreted as the combination of a physical layer and a quantum correlation layer, as depicted in Fig. 1(a) and (b), respectively. The physical layer includes all the tangible components shown in Fig. 1(c). The quantum processor prepares hyperentangled states and distributes them to the end users, which forms the quantum correlation layer shown in Fig. 1(b) and enables the end users communicate with each other. Each user is equipped with a hyperentanglement analysis module to characterize the received polarization and OAM hyperentangled states. The experimental setup of the physical layer is depicted in Fig. 1(c), which consists of a polarization and time-

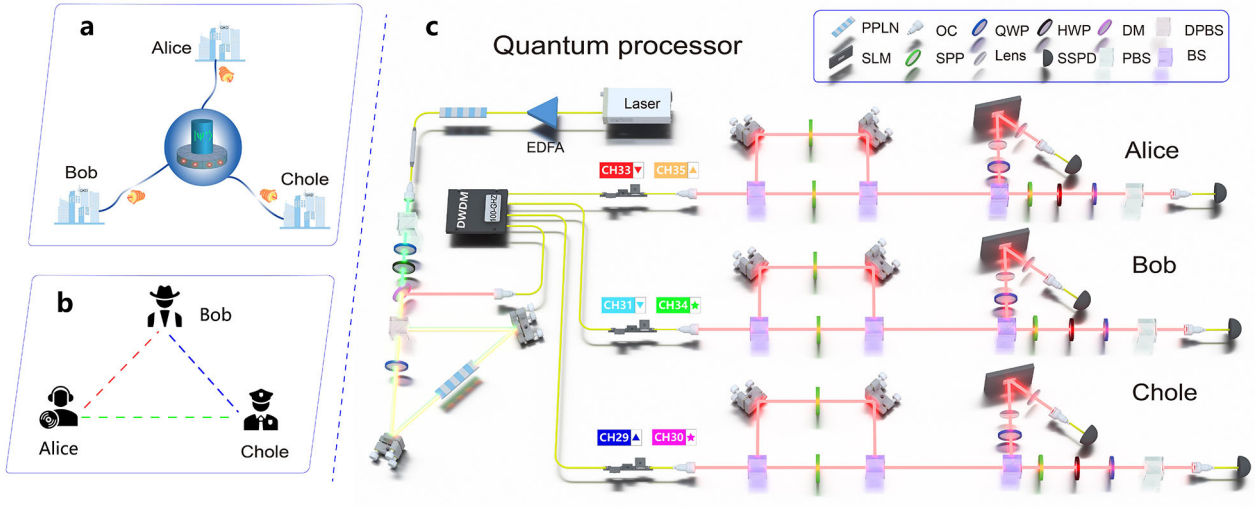

Figure 1 Network architecture and experimental setup. (**a**) Structure of the physical topology of the network. (**b**) Structure of the quantum correlation topology of the network. (**c**) Experimental setup for hyperentangled three-user network. EDFA, erbium doped fiber amplifier; PPLN, periodically poled lithium niobate; OC, optical collimator; QWP, quarter wave plate; HWP, half wave plate; DM, dichroic mirror; DPBS, dual-wavelength polarization beam splitter; SLM, spatial light modulator; SPP, spiral phase plate; PBS, polarization beam splitter; BS, 50:50 beam splitter; DWDM, dense wavelength division multiplexing filter; SSPD, superconducting nanowire single photon detector

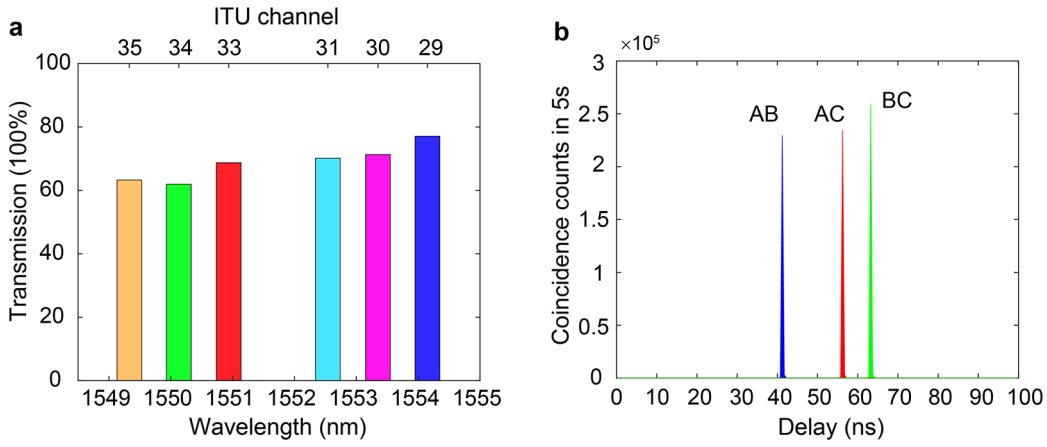

Figure 2 Wavelength multiplexing and temporal cross correlations. (**a**) Independently measure transmission of all the wavelength channels during the network construction. (**b**) Temporal cross-correlations between the time traces of the three users' detectors. AB, Alice-Bob; AC, Alice-Chole; BC, Bob-Chole

energy hyperentangled source, wavelength division demultiplexing and multiplexing modules, and time-energy to OAM entanglement transfer interfaces. A narrow-band continuous-wave laser at 1551.74 nm amplified by an erbium-doped fiber amplifier is frequency doubled in a periodically poled lithium niobate (PPLN) waveguide by second-harmonic generation. The remanent pump laser is suppressed by a wavelength division multiplexing filter with an extinction ratio of 180 dB. The second harmonic is launch into a Sagnac-type setup to bi-directionally pumped another PPLN waveguide through spontaneous parametric down-conversion (SPDC) process, generating polarization Einstein-Podolsky-Rosen pairs in the Bell state: $|\phi^+\rangle_{\text{spin}} = 1/\sqrt{2}(|H\rangle_s|H\rangle_i + |V\rangle_s|V\rangle_i)$. The type-0 SPDC process converts one second harmonic photon at 775.87 nm to a co-polarized signal and idler photons in the telecommunications C-band. The entangled photon pairs are separated from the second harmonic by a dichroic mirror and coupled into a single mode fiber. Owing to the weak dispersion property of PPLN in the telecommunication band, the entangled source spans a full width at half maximum of over 100 nm, covering the whole telecom C- and L-band. The spectrum of the photon pairs is symmetric with respect to the central wavelength of 1551.74 nm and manifests strong frequency correlation due to the photon energy conservation during the SPDC. Considering that time-energy entanglement is an inherent feature of the photon pairs generated via continuous-wave laser pumped SPDC process [41], the quantum states generated in the Sagnac-loop are hyperentangled in polarization and time-energy DOFs.

To implement the fully connected network architecture with three users, a minimum of three quantum correlated photon pairs are required. We use cascaded 100-GHZ DWDM filters to divert the signal and idler photons into six standard international telecommunication union channels, i.e., CH29 to CH31 for signal and CH33 to CH35 for idler. Three DWDM filters are utilized to multiplex two specific channels into one single-mode fiber for each of the three users, ensuring they share a different hyperentangled state with every other user. Figure 2(a) shows the transmissions of the six wavelength channels during the construction of the network architecture, which shows a high transmittance for each channel and predicts a high signal-noise-ratio of the network system. To characterize the performance of the constructed network, we firstly measure the temporal cross-correlation function among three users after the wavelength allocation. The photons are detected by superconducting nanowire single-photon detectors (SSPD) with the detect efficiency of over 80% and dark count rate of less than 40 per second. The detection events of the SSPDs are recorded by a time correlated single-photon counting and the coincidence window during the measurement is set to be 500 ps. Figure 2(b) shows the experimental results of all the quantum correlations among three users. There are three coincidence peaks in the temporal cross-correlation histogram, from which one can identify each entangled pair according to different peak positions. The results mean that any two users share one pair of entangled photons with each other, which indicates a fully connected topological graph has been established.

3 Entanglement transfer from time-energy to OAM DOF

Having confirmed the construction of the fully connected network architecture, we next concentrate on the implementation of hyperentangled state in polarization and OAM DOFs. Before the entanglement transformation, it

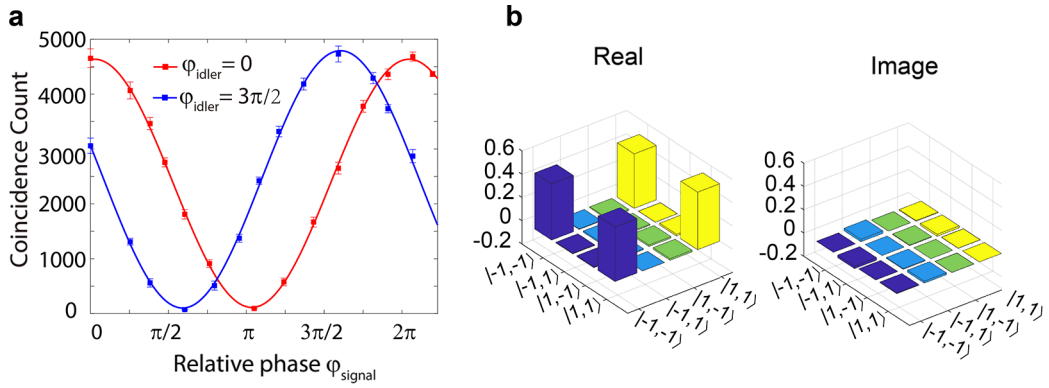

Figure 3 Experimental results for time-energy and OAM entanglement. (**a**) Two-photon interference fringes for time-energy entanglement. Each data is the average coincidence count per second. The error bars represent one standard deviation. (**b**) The real and imaginary parts of the reconstructed density matrix for the OAM entangled state

is important to confirm that the network provide high-quality time-energy entanglement in all available channel pairs. We characterize the time-energy entanglement of each entangled link by measuring the Franson-type interference patterns [42]. Every wavelength multiplexer sends all the received photon channels into an unequal path-length MZI with a path delay Δt of 1 ns controlled by a piezo-actuated displacement platform. At the output of the interferometers, an arrival-time-difference histogram with three peaks can be recorded for each entangled link due to all the possible path combinations. The central peak records the coincidence events that both signal and idler photons pass through the same delay time, corresponding to the state: $1/\sqrt{2}(|t_1\rangle_s|t_1\rangle_i + |t_2\rangle_s|t_2\rangle_i)$, where $|t_1\rangle$ and $|t_2\rangle$ represent the short arm and long arm of the MZIs. We measure the visibilities of Franson-type interference patterns for all entangled links by sweeping the relative phase of one interferometer. Figure 3(a) shows the typical experimental results for the entangled photon pairs shared by Alice and Bob. The two-photon interference fringes under two non-orthogonal phase bases are measured by setting the phase of the MZI in the idler channel at 0 and $3\pi/2$ while varying the phase of the signal. During the measurement, a continuous-wave laser is injected into the MZIs as feedback to stabilize the phase of interferometers. We achieve an average visibility of $V = (96.6 \pm 0.4)\%$ for three entangled links, which strongly suggests time-energy entanglement.

To effectively construct a polarization and OAM hyperentangled network, we transfer the time-energy entanglement to OAM entanglement using three interferometric quantum gates consisting of MZIs and SPPs. Six SPPs with specific topological charge serving as mode shifters are inserted into the two paths of each MZI to form interferometric quantum gates. When the entangled photons with Gaussian mode transmit through the SPP, their azimuthal phase would acquire a phase factor $\exp(i\updownarrow\theta)$, and their profiles become OAM mode of $\updownarrow$, where $\updownarrow$ is an integer and represents the topological charge. Due to the OAM mode conversion, the photons passing through the short path carry an OAM of $\updownarrow_1\hbar$ when leaving the interferometer, while the OAM of the other becomes $\updownarrow_2\hbar$. After precisely adjusting the relative phase of the MZIs, one can obtain a hyperentangled state in OAM and polarization DOFs as the form of:

$$|\psi\rangle = \frac{1}{2}\left(|\updownarrow_1\rangle_s|\updownarrow_1\rangle_i + |\updownarrow_2\rangle_s|\updownarrow_2\rangle_i\right) \otimes \left(|H\rangle_s|H\rangle_i + |V\rangle_s|V\rangle_i\right).$$

With flexibility and adaptability, we experimentally construct the maximally entangled states $|\phi^+\rangle_{\text{orbit}} = 1/\sqrt{2}(|1\rangle_s|1\rangle_i + |-1\rangle_s|-1\rangle_i)$ in OAM DOF for all the entangled links. Three SPPs with an OAM mode of $\updownarrow = 1$ are respectively inserted into the short arms of the MZIs of signal and idler photons while another three SPPs with an OAM mode of $\updownarrow = -1$ are inserted into the long arms. In this way, the polarization and time-energy hyperentangled states are transferred into the polarization and OAM hyperentangled states. Finally, the hyperentangled states are distributed to the end users via free space channels, and each user is equipped with a polarization entanglement detection module and an OAM entanglement detection module to analysis the hyperentanglement.

4 Measurement of OAM and polarization hyperentanglement

To ensure the end users can perform various kinds of quantum tasks, it is vitally important for the quantum processor to provide high-quality entanglement in all available channel pairs. Next, we characterize the performance of the constructed network in term of hyperentanglement

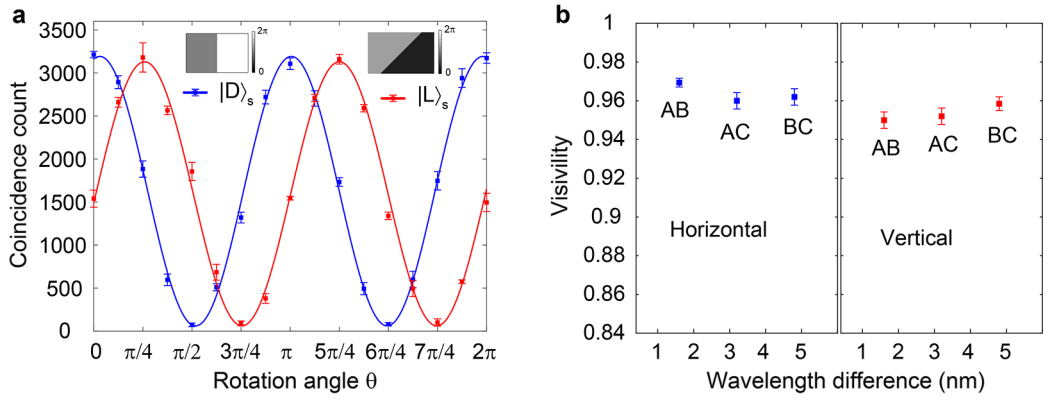

Figure 4 Experimental results for OAM entanglement. (**a**) Typical two-photon interference fringes of the OAM entangled state shared by Alice and Bob. The insets show the phase masks for the projected states $|D\rangle_s = 1/\sqrt{2}(|1\rangle + |-1\rangle)$ and $|L\rangle_s = 1/\sqrt{2}(|1\rangle + i|-1\rangle)$, respectively. Each data is the average coincidence count per second. (**b**) Measured two photon interference visibility for all OAM entangled photon pairs with horizontal and vertical polarization. Each point is the measured result for the entangled state shared by two respective users. The x axis represents the wavelength difference between the channels of the two partner photons. The error bars represent one standard deviation

of polarization and OAM. To demonstrate the versatility and full reconfigurability of our approach, we investigate the OAM entanglement of the correlative links among the three users. The OAM entanglement detection module for each user consists of a spatial light modulator (SLM), a single-mode fiber and a SSPD. The SLMs are utilized to flatten the spiral phase of OAM entangled photons and convert their transverse intensity profile to an Airy-like pattern so that they can be coupled into single mode fiber. Owing to the polarization dependence of the SLMs, a half-wave plate (HWP) is leveraged to switch to detect the horizontally or vertically polarized photons. To fully characterize the established OAM states, we measure the fidelity for each frequency correlated photon pair of the network by performing a quantum state tomography. During the measurement, both the horizontally and vertically polarized photons are successively detected controlled by the HWP. Figure 3(b) shows the typical density matrix reconstructed by using the maximum likelihood estimation for the entangled photons with horizontal polarization shared by Alice and Bob. After reconstructing the density matrix, we calculate the fidelity of the OAM entangled states relative to the ideal Bell state $|\psi_{\text{orbit}}\rangle$ for all available channel pairs of the network. We obtain the average fidelity $F = \langle\psi_{\text{orbit}}|\rho|\psi_{\text{orbit}}\rangle = (96.6 \pm 0.6)\%$, which reveals the high-quality of the constructed OAM states. Then, we further measure the two-photon interference fringes to characterize the OAM entangled states. For this measurement, the OAM-entanglement visibility is measured in two mutually unbiased bases $|D\rangle_s = 1/\sqrt{2}(|1\rangle + |-1\rangle)$ and $|L\rangle_s = 1/\sqrt{2}(|1\rangle + i|-1\rangle)$ by loading the corresponding phase masks to the SLMs for signal photons. Two-photon coincidences are recorded as a function of the rotation angle θ of state $|\theta\rangle_s = 1/\sqrt{2}(e^{i\theta}|1\rangle + e^{-i\theta}|-1\rangle)$ projected to the idler photons. The interference patterns can be obtained when scanning θ from 0 to 2π by the phase masks applied to the SLMs for idler photons. The typical interference patterns for the entangled photons with horizontal polarization between Alice and Bob is shown in Fig. 4(a). Besides, we measured the visibility of all three entangled links for both horizontal and vertical polarization in two mutually unbiased bases mentioned above. The experimental results are shown in Fig. 4(b). The average fringe visibility for all the OAM entangled states is obtained to be $V = (95.9 \pm 0.9)\%$, which exceeds the 71% local bound of the Bell's inequality and convincingly reveals the existence of entanglement. These results prove the OAM entangled network has been constructed well through the scheme of entanglement transfer.

Then, we concentrate on the analysis of polarization entanglement in all available channel pairs. To unequivocally verify quantum mechanical correlations in polarization DOF, a quarter-wave plate (QWP), a HWP, and a cubic PBS are utilized to perform the projected measurements for the polarization entangled states. A SPP is used to eliminate the spatial mode of the correlated photon pairs so that they can be effectively coupled into the single mode fibers. First, the quantum state fidelity of all the polarization-entangled states is measured by using the standard quantum-state tomography technique. After reconstructing their density matrixes using the maximum-likelihood estimation, we calculate the average fidelity of the polarization entangled states compared to the ideal Bell state $|\psi_{\text{spin}}\rangle$ to be $F = \langle\psi_{\text{spin}}|\rho|\psi_{\text{spin}}\rangle = (96.3 \pm 0.8)\%$. Using the standard coincidence measurement technique, we record the two-photon interference fringes in terms of photon coincidence under two nonorthogonal projection bases, H/V and D/A (diagonal and antidiagonal). We fix

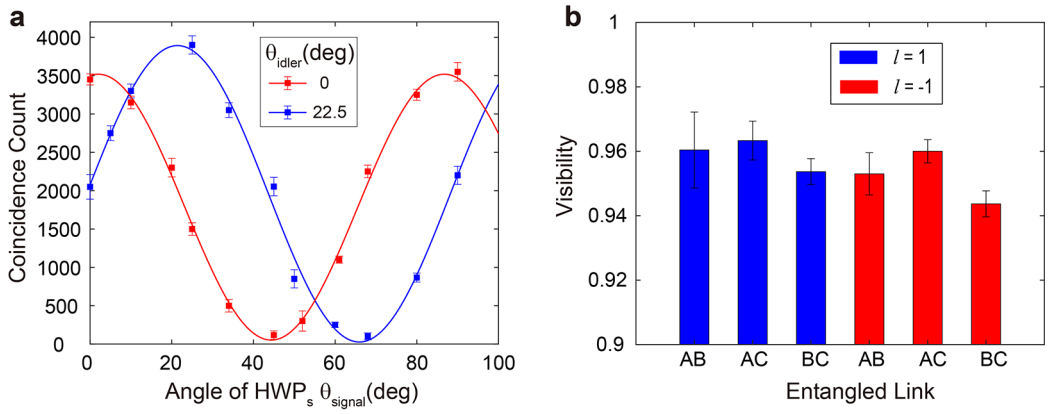

Figure 5 Experimental results for polarization entanglement. (**a**) Typical two-photon interference fringes of the polarization entangled state shared by Alice and Bob. Each data is the average coincidence count per second. (**b**) Measured two-photon interference visibility of the polarization entangled states for all available channel pairs with an OAM mode of $\updownarrow = 1$ and $\updownarrow = -1$, respectively. The error bars represent one standard deviation

the angle of the HWP of idler photons at 0 and 22.5, respectively, and measure the two-photon coincidence count as a function of the HWP rotation angle of signal photons for each entangled photon pair. Figure 5(a) shows the typical interference patterns for polarization entangled state shared by Alice and Bob. We measured the two-photon interference visibility for polarization entanglement of all three entangled photon pairs, with an OAM mode of $\updownarrow = 1$ and $\updownarrow = -1$, in two mutually unbiased bases mentioned above. The experimental results are shown in Fig. 5(b). We obtain an average fringe visibility of $V = (95.6 \pm 0.7)\%$, which exceeds the 71% local bound of the Bell's inequality and reveals the existence of polarization entanglement in all available channel pairs. The results convincingly demonstrate that the polarization-entangled network architecture has been successfully constructed owing to the Sagnac-loop and DWDM technique.

5 Discussion

The experimental results from two experiments above confirm the hyperentanglement nature of the quantum states in all available channel pairs, meaning that our fully-connected network can provide high-quality entangled states in polarization and OAM DOFs simultaneously. In other words, we have successfully realized a proof-of-principle demonstration of a quantum hyperentangled network encoded in polarization and OAM DOFs. It is worth noting that the time-energy and OAM DOFs belong to high dimensional Hilbert space. One can prepare the high-dimensional OAM entangled states through entanglement transfer from time-energy to OAM DOF by inserting relative SPPs into multi-arm unbalanced interferometers, which is promising in constructing a high-dimensional OAM entangled network. Besides, the scale of the network can be easily expanded by multiplexing more wavelength channels into one transmission link using DWDM technique, and new users can be added to the network architecture without changing the users' hardware while maintaining the network's performance. When the number of end users grows to be large, the quantum system for a fully-connected hyperentangled network would be complicated, which makes it difficult to improve the security distance of the network. At this time, powerful quantum repeaters are necessary to implement the functionality of a quantum Internet [21] with multiusers. To date, it is still challenging to achieve a practical quantum repeater. One solution is to use secure-repeater network based on QSDC [43], which provides a way of quantum interconnection in the future quantum Internet.

6 Conclusion

We implement a hyperentangled multiuser network encoded in polarization and OAM DOFs with a fully connected network architecture by using the DWDM and entanglement transfer technique. During the experiment, three hyperentangled states in polarization and time-energy DOFs from a Sagnac-type setup are multiplexed into three single mode fibers to form the fully connected network architecture. Then, three interferometric quantum gates consisting of a MZI with two SPPs inserted in different paths are utilized for quantum entanglement transfer from time-energy to OAM DOF. The two-photon interference visibility is measured to be higher than 95% for both polarization and OAM entanglement, revealing a high quality of the hyperentanglement in polarization and OAM DOFs of the constructed network. The scheme based on entanglement transfer has potential applications in high-dimensional quantum communication tasks since the time-energy and OAM DOFs belong to high dimensional Hilbert space. Our approach can provide a novel

way to construct a large-scale hyperentangled network that can support various kinds of multiuser quantum communication tasks, such as multi-DOF quantum entanglement swapping, superdense coding, and teleportation.

Acknowledgements
Not applicable.

Funding
This work is supported in part by the National Natural Science Foundation of China (Grant Nos. 12192252 and 12074155), The Foundation for Shanghai Municipal Science and Technology Major Project (Grant No. 2019SHZDZX01-ZX06), and Jiangxi Provincial Natural Science Foundation (Grants No. 20212ACB201004, Grant No. 20202ACBL211003). Open Access funding provided by Shanghai Jiao Tong University.

Availability of data and materials
The data and materials can be requested from corresponding author via e-mail.

Declarations

Ethics approval and consent to participate
Not applicable.

Consent for publication
Not applicable.

Competing interests
The authors declare no competing interests.

Author contributions
XC led the project since its conception and supervised all experiments. YH, ZQ and YY performed the experiment and data analysis. All authors participated in discussions of the results. YH prepared the manuscript with assistance from all other co-authors. YL, YZ and XC provided revisions. All authors read and approved the final manuscript.

Author details
[1]State Key Laboratory of Advanced Optical Communication Systems and Networks, School of Physics and Astronomy, Shanghai Jiao Tong University, Shanghai 200240, China. [2]Department of Physics, Shanghai Key Laboratory of Materials Protection and Advanced Materials in Electric Power, Shanghai University of Electric Power, Shanghai 200090, China. [3]Shanghai Research Center for Quantum Sciences, Shanghai 201315, China. [4]Collaborative Innovation Center of Light Manipulation and Applications, Shandong Normal University, Jinan 250358, China.

Received: 10 April 2023 Revised: 10 May 2023 Accepted: 16 May 2023
Published online: 24 May 2023

References

1. Horodecki R, Horodecki P, Horodecki M, Horodecki K (2009) Quantum entanglement. Rev Mod Phys 81(2):865
2. Gisin N, Ribordy G, Tittel W, Zbinden H (2002) Quantum cryptography. Rev Mod Phys 74(1):145
3. Gisin N, Thew R (2007) Quantum communication. Nat Photonics 1(3):165–171
4. Erhard M, Krenn M, Zeilinger A (2020) Advances in high-dimensional quantum entanglement. Nat Rev Phys 2(7):365–381
5. Li ZD, Zhang R, Yin XF et al (2019) Experimental quantum repeater without quantum memory. Nat Photonics 13(9):644–648
6. Bouwmeester D, Pan JW, Mattle K, Eibl M, Weinfurter H, Zeilinger A (1997) Experimental quantum teleportation. Nature 390(6660):575–579
7. Takesue H, Dyer SD, Stevens MJ, Verma V, Mirin RP, Nam SW (2015) Quantum teleportation over 100 km of fiber using highly efficient superconducting nanowire single-photon detectors. Optica 2(10):832–835
8. Liu S, Lou Y, Chen Y, Jing J (2022) All-optical entanglement swapping. Phys Rev Lett 128(6):060503
9. Sun QC, Jiang YF, Mao YL et al (2017) Entanglement swapping over 100 km optical fiber with independent entangled photon-pair sources. Optica 4(10):1214–1218
10. Treiber A, Poppe A, Hentschel M et al (2009) A fully automated entanglement-based quantum cryptography system for telecom fiber networks. New J Phys 11(4):045013
11. Liu X, Yao X, Xue R et al (2020) An entanglement-based quantum network based on symmetric dispersive optics quantum key distribution. APL Photon 5(7):076104
12. Kwek LC, Cao L, Luo W et al (2021) Chip-based quantum key distribution. AAPPS Bull 31:15
13. Long GL, Liu XS (2002) Theoretically efficient high-capacity quantum-key-distribution scheme. Phys Rev A 65(3):032302
14. Wang T, Han X, Liu S et al (2022) Manipulation and enhancement of asymmetric steering via down-converted nondegenerate photons. AAPPS Bull 32(1):33
15. Wang S, Yin ZQ, He DY et al (2022) Twin-field quantum key distribution over 830-km fibre. Nat Photonics 16(2):154–161
16. Li W, Zhang L, Tan H et al (2023) High-rate quantum key distribution exceeding 110 Mb s^{-1}. Nat Photonics 17:416–421
17. Xu F, Ma X, Zhang Q et al (2020) Secure quantum key distribution with realistic devices. Rev Mod Phys 92(2):025002
18. Simon C (2017) Towards a global quantum network. Nat Photonics 11(11):678–680
19. Chen YA, Zhang Q, Chen TY et al (2021) An integrated space-to-ground quantum communication network over 4600 kilometres. Nature 589(7841):214–219
20. Lingaraju NB, Lu HH, Seshadri S, Leaird DE, Weiner AM, Lukens JM (2021) Adaptive bandwidth management for entanglement distribution in quantum networks. Optica 8(3):329–332
21. Wehner S, Elkouss D, Hanson R (2018) Quantum Internet: a vision for the road ahead. Science 362(6412):eaam9288
22. Degen CL, Reinhard F, Cappellaro P (2017) Quantum sensing. Rev Mod Phys 89(3):035002
23. Wang S, Chen W, Yin ZQ et al (2014) Field and long-term demonstration of a wide area quantum key distribution network. Opt Express 22(18):21739–21756
24. Pan D, Lin Z, Wu J et al (2020) Experimental free-space quantum secure direct communication and its security analysis. Photon Res 8(9):1522–1531
25. Pan D, Song XT, Long GL (2023) Free-space quantum secure direct communication: basics, progress, and outlook. Adv Dev Instrum 4:0004
26. Wengerowsky S, Joshi SK, Steinlechner F, Hübel H, Ursin R (2018) An entanglement-based wavelength-multiplexed quantum communication network. Nature 564(7735):225–228
27. Joshi SK, Aktas D, Wengerowsky S et al (2020) A trusted node–free eight-user metropolitan quantum communication network. Sci Adv 6(36):eaba0959
28. Huang Z, Joshi SK, Aktas D et al (2022) Experimental implementation of secure anonymous protocols on an eight-user quantum key distribution network. npj Quantum Inf 8(1):25
29. Kim JH, Chae JW, Jeong YC et al (2022) Quantum communication with time-bin entanglement over a wavelength-multiplexed fiber network. APL Photon 7(1):016106
30. Barasiński A, Černoch A, Lemr K (2019) Demonstration of controlled quantum teleportation for discrete variables on linear optical devices. Phys Rev Lett 122(17):170501
31. Barreiro JT, Wei TC, Kwiat PG (2008) Beating the channel capacity limit for linear photonic superdense coding. Nat Phys 4(4):282–286
32. Williams BP, Sadlier RJ, Humble TS (2017) Superdense coding over optical fiber links with complete Bell-state measurements. Phys Rev Lett 118(5):050501
33. Zhong HS, Wang H, Deng YH et al (2020) Quantum computational advantage using photons. Science 370(6523):1460–1463
34. Liu S, Lou Y, Jing J (2020) Orbital angular momentum multiplexed deterministic all-optical quantum teleportation. Nat Commun 11(1):3875
35. Wang W, Zhang K, Jing J (2020) Large-scale quantum network over 66 orbital angular momentum optical modes. Phys Rev Lett 125(14):140501
36. Huang Y, Li Y, Qi Z, Feng J, Zheng Y, Chen X (2022) A two-way photonic quantum entanglement transfer interface. npj Quantum Inf 8(1):8
37. Zeitler CK, Chapman JC, Chitambar E, Kwiat PG (2022) Entanglement verification of hyperentangled photon pairs. Phys Rev Appl 18(5):054025

38. Ecker S, Sohr P, Bulla L, Huber M, Bohmann M, Ursin R (2021) Experimental single-copy entanglement distillation. Phys Rev Lett 127(4):040506
39. Chapman JC, Graham TM, Zeitler CK, Bernstein HJ, Kwiat PG (2020) Time-bin and polarization superdense teleportation for space applications. Phys Rev Appl 14(1):014044
40. Zhao TM, Ihn YS, Kim YH (2019) Direct generation of narrow-band hyperentangled photons. Phys Rev Lett 122(12):123607
41. Huang Y, Feng J, Li Y et al (2022) High-performance hyperentanglement generation and manipulation based on lithium niobate waveguides. Phys Rev Appl 17(5):054002
42. Franson JD (1989) Bell inequality for position and time. Phys Rev Lett 62(19):2205
43. Long GL, Pan D, Sheng YB et al (2022) An evolutionary pathway for the quantum Internet relying on secure classical repeaters. IEEE Netw 36(3):82–88

Publisher's Note